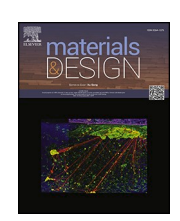
ELSEVIER

Contents lists available at ScienceDirect

Materials & Design

journal homepage: www.elsevier.com/locate/matdes





Design strategy for 3D layer-to-layer angle interlock woven composites

Elena Sitnikova^{a,*}, Mingming Xu^b, Weiyi Kong^c, Shoufeng Hu^d, Shuguang Li^a

- ^a Faculty of Engineering, The University of Nottingham, Nottingham NG8 1BB, UK
- ^b School of Science, Harbin Institute of Technology (Shenzhen), Shenzhen 518055, China
- ^c TaiHang Laboratory, Tianfu New Area, Chengdu, Sichuan Province 610213, China
- ^d AECC Commercial Aircraft Engine Co., LTD, Shanghai 200241, China

ARTICLE INFO

Keywords: 3D woven composite Mechanical properties Analytical modelling Elastic characterisation Key Properties of Weave (KPOWs)

ABSTRACT

A design strategy for 3D layer-to-layer angle interlock woven composites has been established by employing a set of three key properties of the weave (KPoWs): the global fibre volume fraction, the interlocking angle and the ratio of the weft tow volume to the warp tow volume. Using analytically derived expressions of the KPoWs, their variation trends relative to the manufacturing parameters have been revealed. At the same time, via a range of systematic computational material characterisation exercises, the KPoWs were shown to be sufficient for representing the woven reinforcement as far as the elastic behaviour predictions are concerned, because the effective elastic properties were found to follow consistent variation trends with the KPoWs. As a result, through use of KPoWs, manufacturing parameters have been associated with the effective elastic properties in a systematic manner. This offer means for obtaining a desirable elastic behaviour of 3D woven composites via variation of their internal architecture. The design method developed is the alternative to trial-and-error-based selection method conventionally adopted for this type of materials. As an example of application of the proposed method, a woven composite with balanced weft and warp properties has been designed.

1. Introduction

After decades of research into 3D woven textile composites, substantial volume of knowledge has been accumulated regarding their manufacture [1], modelling [2,3] and performance [4,5]. While composites of this type are already being applied in manufacturing of high-performance components, the best known of which are the fan blades and the containment casing of Leap-1C engine [6], there are still no clearly defined design guidelines for these materials.

A distinctive feature of 3D woven composites is that their internal construction can be varied significantly by altering the arrangement of the tows in the weave. The internal construction, in turn, affects the mechanical performance of 3D woven composites. Therefore, by changing the geometry of the tows and their layout, virtually infinite variety of woven architectures can be obtained that would deliver very different mechanical behaviour. The task of the designer would be to navigate this variety of woven reinforcements by making an informed decision based on some established design guidelines. In absence of such guidelines, this task is formidable at present.

The design of 3D woven composites for the mechanical performance is a topic hardly ever addressed in the literature, despite its high importance. In the present paper, the design is understood as means of selecting the material configuration that would deliver a desired mechanical behaviour. For design of the composites to be possible, one should have good understanding of the association between the internal architecture and the mechanical behaviour. A simple example is design of conventional laminated composites based on unidirectional plies. A typical route that is followed in laminate design is to consider the quasiisotropic composite as an initial configuration, based on which the desired performance under a given type of load is obtained by adding more plies to reinforce the material [7], for example, adding more $\pm 45^\circ$ plies to increase the shear stiffness and strength. There is clear lack of an equivalent design method for 3D woven composites, even for designing their elastic behaviour, let alone for tackling more sophisticated mechanical behaviour, such as damage and failure.

The most popular method of establishing the relationship between the reinforcement architecture and the mechanical behaviour of 3D woven composites is the comparative experimental studies [8,9]. Comparison can be between composites based on different types of reinforcement, as in [10], where both orthogonal and angle interlock composites were tested, or in [11], where 2D and 3D reinforcements effects were compared. Alternatively, reinforcement geometry features

E-mail address: elena.sitnikova@nottingham.ac.uk (E. Sitnikova).

^{*} Corresponding author.

can be varied for the same type of composite, as in [12,13], where the effect of binder yarn sizes [12] and bias yarn content [13] on mechanical behavior of orthogonal interlock composites were studied. While the experimental findings can be reasonably informative, they are by far neither sufficiently comprehensive nor systematic. Given the variety of types of reinforcements, basing the design on the experiments alone would be highly impractical.

Recently, there has been a growing interest in development of design methods for woven composites using computational means. This includes use of optimisation algorithms as design tools for 2D [14,15] and 3D woven composites [16], and can also involve use of the neural network methodology if more sophisticated material behaviours are targeted [17]. The main issue of this type of approaches is the inevitable complexity of their formulation and implementation. In addition to definition of the optimisation problem itself, which requires welldefined design parameters and constraints, the formulation has to incorporate material characterisation procedures, be it finite element analysis or any other type of homogenisation, which on its own can be a challenge. Interpretation and verification of the results of such optimisation is yet another issue, given the complexity of the problem. While the optimisation as a method of design can be a powerful design tool, the elastic behaviour of 3D woven composites can be controlled and designed using much simpler means that will be established as the main outcome of the present paper.

In modelling and computational characterisation of 3D woven composites, the biggest challenge is the representation of their sophisticated architecture in models so that the predictive capability of the models could be established and improved. Variation of the geometry of the tows along their paths is the modelling aspect that started to receive a lot of attention in recent years. Methods of reproducing realistic geometries of the fibre tows in orthogonal interlock composites have been reported in [18,19], while the varying geometry of layer-to-layer angle interlock composite has been modelled in [20,21]. Additional cause of geometric non-uniformity in layer-to-layer angle interlock reinforced composites considered in [22] was the twisting applied to a preform during the manufacture so it would reproduce a complex geometry of a fan blade in an aero-engine. While improvement of predictive capability is certainly important, building up the complexity of the models is usually detrimental to development of the design methodology. Models delivering highly detailed representation of the composite architecture are often impractical in application to design. Specifically, in the design of conventional laminated composites a comparable example is use of classical laminate theory [23]. While high order theories or even 3D models for laminate analysis are available, the classical laminate theory still remains the most popular analysis tool even though it involves simplifying assumptions. Furthermore, for 3D woven composites, the localised variations of the geometry are not truly designable features in a sense that they cannot be prescribed and controlled in a straightforward manner. Once again drawing analogy to laminate design, one assumes its idealised construction when carrying out the design exercise, neglecting potential influence on the mechanical performance of fibre misalignment in the ply, or ply misalignment in the laminate.

For composites design to be feasible, as the first step, one needs to identify the designable parameters. Ideally, the designable parameters should be directly associated with the manufacturing ones, so that the design outcomes could be easily interpreted by the manufacturers. For example, for composite laminates, such parameters are the orientation, the number and the thickness of the plies. In modern 3D woven composites research, parametrisation of their complex reinforcement architecture primarily involves their geometric features, such as dimensions of tow cross-sections and spacing between the tows. Specifically, popular 3D woven architecture construction and analysis tools, Texgen [24] and WiseTex [25], use geometric parameters of this kind as an input. The issue has been explicitly flagged up in [26] that such parameters are unsuitable for applications in serious design exercises, because they merely quantify some of the weave features while bearing

no relevance to manufacturing. A solution, also offered in [26], was to adopt the manufacturing-based parameters, referred to as the controllable parameters, that were shown to comprehensively define the geometry of the woven composites of layer-to-layer angle interlock architecture, assuming their idealised construction. Treating unit cell (UC) modelling as the design tool, a design cycle for 3D woven composites was formulated and shown to be equivalent to that for the conventional laminates.

Since controllable parameters represent the manufacturing characteristics of the weave, they are the natural means for prescribing variations of the weave. However, to realise the design cycle, one should understand how the designable parameters would affect the mechanical behaviour, when altered. It is not clear how to establish such association, especially given that the number of controllable parameters identified in [26] was 10, which is clearly too many if one needs to relate all of them to the mechanical behaviour.

An even more important consideration is systematic selection of valid combinations of controllable parameters. Assigning them with arbitrary values could easily result in configurations where the total fibre volume fraction will either be unreasonably high or too low. This, in fact, is the major conceptual difference between the laminate design and the design of the textile composites in general. Specifically, for the former, practical fibre volume fraction is usually achieved naturally because it is controlled mostly through the prepreg employed. However, in woven composites, the global fibre volume fraction is a derived property, and special measures should be taken in design exercises to ensure that it remains reasonable.

The fibre volume fraction is known to have a profound effect on the overall mechanical performance of the composites. For 3D woven composites, there are two other properties of similar significance. One is the *interlocking angle*, defined as the slope of the inclined part of the warp tow [27]. It is generally acknowledged that waviness, or the crimp, of the warp tows affects the properties of composite along the warp direction. Another property is the ratio of the weft to the warp tow volumes, henceforth referred to as the *tow ratio* for simplicity. Effectively, it reflects a relative content of different types of tows. While there is no conventional definition for it, it is often referred to in some form in the existing research on woven composites [21,28]. Together, the global fibre volume fraction, the interlocking angle and the tow ratio will be referred to as key properties of the weave (KPoWs) in the present paper.

Based on previously established parameterisation, these properties will be derived explicitly. They will be shown to reflect contribution of all the controllable parameters. It will be shown that the elastic properties of the composites follow specific variation trends with respect to the KPoWs. Topped it up with considerations of topological construction and its effect on the elastic response of the composite, the complete practical design cycle for 3D woven composites will be established as the main outcome of the present paper.

2. Parametrisation of 3D woven composites

Parametrisation of 3D woven composites of layer-to-layer angle interlock architecture has been originally reported in [27]. This choice of woven architecture has been explained in [26] and, prior to that, in [29], where it was elaborated that presence of warp tows inclined to the transverse direction is beneficial in terms of resisting transverse loading, such as the lateral impact. A parametrisation strategy was to describe the composites architecture via a finite set of parameters, thus unifying definition of the wide variety of architectures. The parametrisation in [27] was taken a step closer to practical applications in [26] by relating the geometric properties to the manufacturing-based parameters and, through this, ensuring the feasibility of the 3D woven composites design. The accuracy in predicting the experimental data delivered by these idealised models has been assessed in [26] employing six woven composites of different constituents and reinforcement architectures.

Since parametrisation offers a foundation to the subsequent

derivations of the KPoWs in Section 3, it will be briefly covered in the present section, tailoring its formulation to a form that will streamline its application in design exercises.

2.1. Parametrisation of the tow cross-section

Seven geometric parameters define the geometry of the weave [27]. Six of them are associated with the geometry of the tow cross-sections, the warp and the weft ones. The remaining one is the spacing between the weft tows, D_{weft} , as is marked in Fig. 1(b). The cross-section has been idealised by a rectangle with two semi-ellipses on the sides, as shown in Fig. 1(a). It is defined by the height, H = 2b, the width, W, and the measure of roundness, γ , expressed as

$$\gamma = \frac{2a}{W},\tag{1}$$

where a is the length of the horizontal semi-axis of the elliptical part of the cross-section. Parameter γ can vary in a range (0,1], where $\gamma \approx 0$ corresponds to nearly rectangular cross-section profile, while at $\gamma = 1$ the cross-section is elliptical.

2.2. Parametrisation of the weave

The controllable parameters associated with the weave were identified in [26]. Two of them were the weft and the warp tow densities, denoted as p_{warp} and p_{weft} , respectively. Tow density is a conventional weaving parameter in preform manufacturing, and it is often defined as the number of tows in 1 cm of fabric. To retain consistency with its conventional manufacturing definition, it will be given in cm⁻¹ throughout this paper. As a result, a factor of 10 will appear in some of the derived expressions to keep a consistent unit system. Additionally, a group of three controllable parameters associated with through-the-thickness construction was employed in [26]. In the present work, it will be replaced with a single parameter

$$H_{UC} = H_{warp} + H_{weft}, (2)$$

where H_{UC} is a height of a single unit cell of the woven composite, based on which the thickness of the composite panel can then be recovered, when needed, as a multiple of H_{UC} . Effectively, H_{UC} reflects density of tows through the thickness of the composite: for a given thickness, the more H_{UC} it contains, the denser is the tow packing through the thickness. Because of that, H_{UC} will also be referred to as the tow density, even though its dimension is different to those of p_{warp} and p_{weft} .

With the exception of H_{UC} , geometric parameters have been expressed in terms of the controllable parameters in [26] as follows

$$W_{warp} = \frac{10}{p_{warp}},\tag{3}$$

$$H_{warp} = \frac{A_{warp}}{W_{warp} \left(\gamma_{warp} \left(\frac{\pi}{4} - 1\right) + 1\right)} = \frac{A_{warp} p_{warp}}{10\Gamma_{warp}},\tag{4}$$

$$H_{weft} = H_{UC} - H_{warp} = H_{UC} - \frac{p_{warp} A_{warp}}{10 \Gamma_{warp}},\tag{5}$$

$$W_{weft} = \frac{A_{weft}}{H_{weft} \left(\gamma_{weft} \left(\frac{\pi}{4} - 1 \right) + 1 \right)} = \frac{10 \Gamma_{warp} A_{weft}}{\left(10 \Gamma_{warp} H_{UC} - A_{warp} p_{warp} \right) \Gamma_{weft}}, \tag{6}$$

and

$$D_{weft} = \frac{10}{p_{weft}} - W_{weft} = \frac{10}{p_{weft}} - \frac{10\Gamma_{warp}A_{weft}}{\left(10\Gamma_{warp}H_{UC} - A_{warp}p_{warp}\right)\Gamma_{weft}},\tag{7}$$

where

$$\Gamma_{warp} = \left(\gamma_{warp} \left(\frac{\pi}{4} - 1 \right) + 1 \right), \quad \Gamma_{weft} = \left(\gamma_{weft} \left(\frac{\pi}{4} - 1 \right) + 1 \right)$$
 (8)

and A_{weft} and A_{warp} are the cross-sectional areas of the weft and the warp tows, respectively. In [26], a tow cross-sectional area, A, was defined in terms of the controllable parameters as

$$A = \frac{\pi d_f^2 F}{4V_f},\tag{9}$$

where d_f is a filament diameter, F is the filament count and V_f the intratow fibre volume fraction. In general, all of them can be different in the warp and the weft tows and, therefore, the weft and the warp crosssectional areas can also be different. From the numerical modelling perspective, when the fibre tows are treated as monolithic material, it is irrelevant which of controllable parameters in Eq. (9) are responsible for the change in cross-sectional area. For example, the tow cross-sectional area could change if the number of filaments or a filament diameter is altered, or the combination of the two. However, in meso-scale modelling, as is employed in the present paper, all that matters is the change in cross-section, and not the cause of it. Because of that, henceforth, the warp and the weft tow cross-sectional areas will be treated as two controllable properties reflecting the combined contribution of controllable parameters associated with them. Note that in the present paper, term 'property' in relation to woven architecture reflects a characteristic of the weave that is expressed as function of the controllable parameters.

In addition to geometric parametrisation, five integer topological parameters were employed in [27] to define the arrangement of the tows relative to each other. Three of them, n_{steep} , n_{deep} and n_{skip} , marked in Fig. 2(a) and (b), define the path of a warp tow as it crosses the columns of the weft tows. Relating paths of the warp tows to respective topological parameter values in Fig. 2(a) and (b), the nature of changes associated with each topological parameter can be understood. Topological parameter n_{step} defines the extent of shifting of the adjacent warp

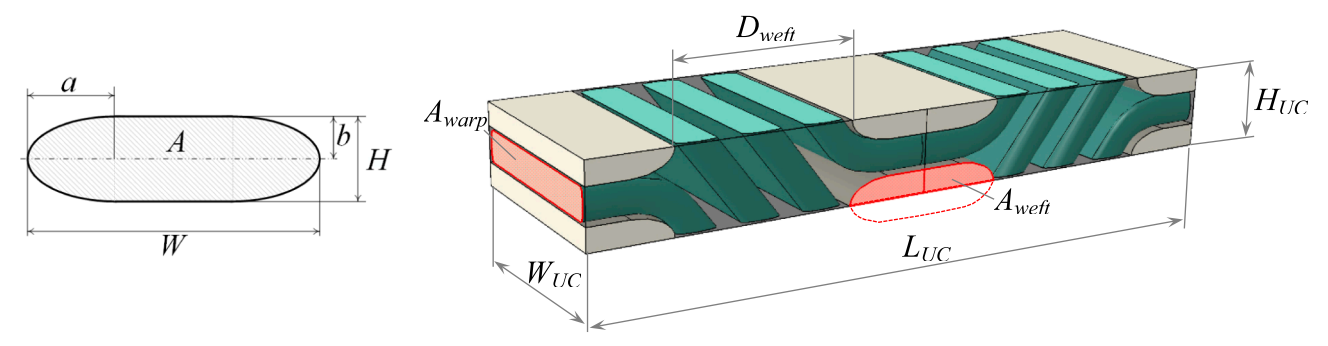


Fig. 1. Geometric properties and parameters of (a) the tow cross-section and (b) the unit cell.

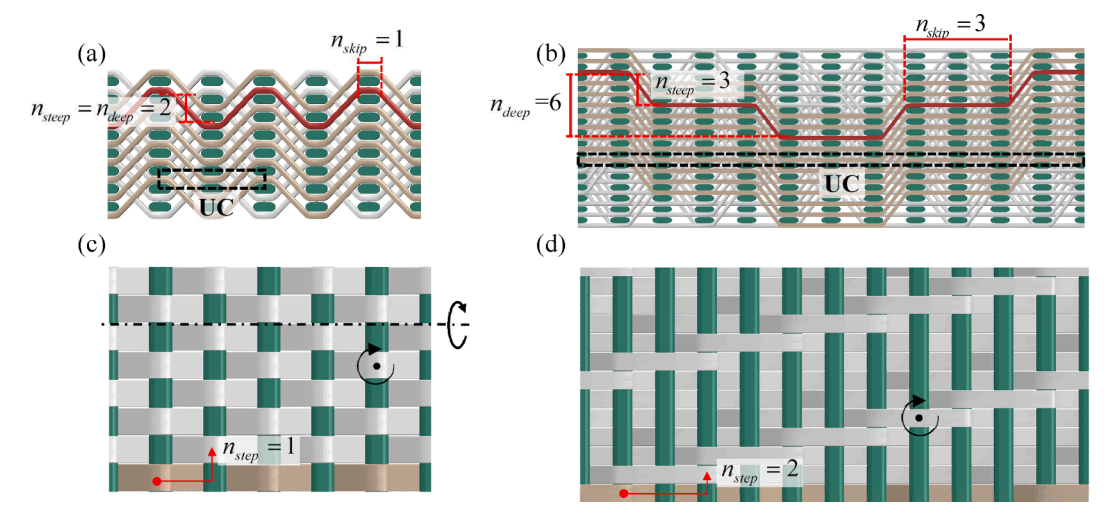


Fig. 2. Topological parameters n_{steep} , n_{deep} and n_{skip} specified on cross-sectional views of two different weaves (a) and (b); topological parameter n_{step} specified on the top view of the same weaves (c) and (d).

tows relative to each other when forming an interlocking pattern, as is illustrated by Fig. 2(c) and (d). Further details related to definition of these parameters can be found in [27].

The remaining topological parameter, n_{offset} describes variations of the weave architecture were alternating columns or layers of weft tows were shifted relative to each other. While such configurations are also practical, their topological variations are more limited in a sense that some of the topological parameters become void in presence of the offset, namely, n_{skip} for the weave with the vertical offset, and n_{skip} and n_{skep} for the weave with the horizontal offset. Therefore, the present work will be focused on establishing the design functionality for the weave with no offset as the benchmark type of layer-to-layer angle interlock, although the same design principles could be applicable to the weaves with an offset.

3. Key properties of the weave

The design methodology that is being developed relies on availability of a computationally efficient method for calculating the KPoWs. Explicit derivation of the KPoWs as functions of controllable parameters readily delivers such a method, as will be elaborated in the present section.

3.1. Derivation of the key properties of the weave

The 3D woven composite parametrisation established in [27] offers convenient means for deriving the KPoWs explicitly. While the geometry of woven reinforcement is complex in general, its idealisation and representation by a parametrised unit cell makes analytical derivation of the KPoWs possible. Such derivations, while requiring substantial effort, are purely geometric exercise whose only purpose is to deliver the explicit expressions of the KPoWs. Therefore, their details are provided

in the Supplementary File document (available online), and only the final expressions of KPoWs are given below.

The interlocking angle, marked as θ in Fig. 3, is determined as [23]

$$tan\theta = \frac{H_{weft}}{W_{weft}\gamma_{weft}}\cot\varphi_0,$$
(10)

where φ_0 is the parameter in the parametric equation of the ellipse at which the warp tow becomes straight. The point at which such transition takes place is marked in Fig. 3. This parameter is defined in a range $\varphi_0 \in$

 $\left(0,rac{\pi}{2}
ight)$ and it is determined from a transcendental equation for arphi given as

$$-(n_{steep} - 1)\left(\frac{H_{warp}}{H_{weft}} + 1\right)\sin\varphi + \left(\frac{D_{weft}}{W_{weft}\gamma_{weft}} + 1\right)\cos\varphi - \frac{H_{warp}}{H_{weft}}\sqrt{\sin^2\varphi + \left(\frac{H_{weft}}{W_{weft}\gamma_{weft}}\right)^2\cos^2\varphi} - 1$$

$$= 0 \tag{11}$$

employing a root-finding method such as Newton iterations.

The global fibre volume fraction has been obtained the function of the controllable properties and parameters as

$$V_f^{global} = \frac{A_{weft} p_{weft}}{10 H_{UC}} V_{f,weft} + \frac{A_{warp} p_{warp}}{10 H_{UC}} k V_{f,warp}, \tag{12}$$

where $V_{f,weft}$ and $V_{f,warp}$ are the intra-tow fibre volume fractions in the weft and the warp tows, respectively.

The tow ratio has been derived as

$$\frac{V_{weft}}{V_{warp}} = \frac{A_{weft}p_{weft}}{A_{warp}p_{warp}k},\tag{13}$$

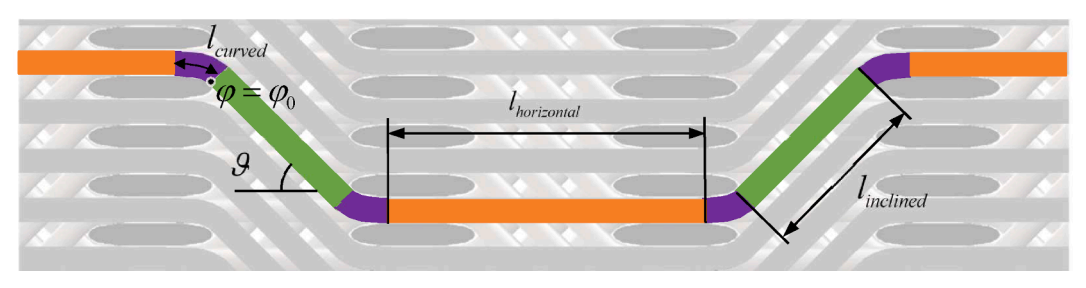


Fig. 3. Building blocks of a warp tow within a UC of topology corresponding to $n_{skip} = 2$, $n_{steep} = n_{deep} = 3$.

where V_{weft} is the total volume of the weft tows and V_{warp} is the total volume of the warp tows within a unit cell. Non-dimensional property k in Eqs. (12) and (13) is expressed as

$$k = \frac{p_{weft}}{10n_{skin}} (l_{horizontal} + l_{inclined} + 2l_{curved})$$
(14)

where $l_{horizontal}$ and $l_{inclined}$ are the lengths and l_{curved} is the arc length of warp tow segments as marked in Fig. 3. Their explicit expressions have been obtained as

$$l_{horizontal} = n_{skip} (W_{weft} + D_{weft}) - \gamma_{weft} W_{weft} - D_{weft}$$
(15)

erroneous prediction of the warp tow volume, since the interlocking angle is involved in its calculation through parameter φ_0 .

3.2. Designable parameters

To facilitate the demonstration and discussion of the design scheme, and to directly relate it to practical applications, woven composite that has been previously characterised and tested in [26] will be employed as the benchmark case. It was based on TZ800H fibre tows [31], and a complete set of parameters defining its internal architecture is given in Table 1.

Note that the values of the intra-tow fibre volume fractions given in Table 1 were different from those used in [26]. While some evidence has

$$l_{inclined} = \sqrt{\frac{\left(\left(W_{weft}\gamma_{weft} + \frac{H_{warp}H_{weft}}{r}\right)\cos(\varphi_{0}) - W_{weft}\gamma_{weft} - D_{weft}}{r}\right)^{2} + \left(\left(H_{weft} + \frac{H_{warp}W_{weft}\gamma_{weft}}{r}\right)\sin(\varphi_{0}) + \left(n_{steep} - 1\right)\left(H_{warp} + H_{weft}\right)\right)^{2}}$$

$$(16)$$

$$\begin{split} l_{curved} &= \frac{H_{warp}}{2} \left(\frac{\pi}{2} \right. \\ &- \arctan \left(\frac{W_{weft} \gamma_{weft}}{H_{weft}} \tan \varphi_0 \right) \left. \right) + \frac{H_{weft}}{2} \left(\int_0^{\frac{\pi}{2}} \sqrt{1 - m \sin^2 \varphi} \, d\varphi \right. \\ &- \int_0^{\varphi_0} \sqrt{1 - m \sin^2 \varphi} \, d\varphi \right) \end{split} \tag{17}$$

where

$$m = 1 - \left(\frac{W_{weft}\gamma_{weft}}{H_{weft}}\right)^{2} \text{ and } r$$

$$= W_{weft}\gamma_{weft}\sqrt{\sin^{2}(\varphi_{0}) + \left(\frac{H_{weft}}{W_{weft}\gamma_{weft}}\right)^{2}\cos^{2}(\varphi_{0})}$$
(18)

The derived expressions for calculating the interlocking angle (11), the global fibre volume fraction (12) and the tow ratio (13) are still reasonably complex, and some of them cannot be fully resolved analytically. However, they can easily be implemented as a short MATLAB script [30], thus streamlining the calculation procedure. The only required input are the controllable parameters, while all the intermediate calculation steps, including solution of transcendental equation (11) and calculation of the elliptic integrals in Eq. (17) will be carried out automatically. The MATLAB script has been extensively verified by comparing its outputs with those obtained from Abaqus when carrying out the unit cell analysis for the same composite configurations. Specifically, Abaqus has its own functionality to evaluate the volume of the shapes, which is completely independent of their calculations carried out with MATLAB script. As a verification, the total volumes of the weft and warp tows were output from Abaqus along with the volume of the UC and they were compared with their counterparts from MATLAB calculations. Such comparison has been carried out for multiple characterisation exercises, including those of composite configuration analysed in the sections below. The relative differences between the respective values calculated using these two methods were well below 1 % and they were due to the numerical rounding errors. This also indirectly verifies accuracy of calculation of the interlocking angle, because any error made in its calculation would inevitably cause

been presented in [26] that these parameters can in fact be considered reasonably constant for 3D woven composites, given lack of conclusive studies for complete justification of this assumption, they were measured here for TZ800H composite.

Specimen preparation and imaging followed the procedure detailed in [26]. The micrographs of the warp and the weft tow cross-sections were converted to bitmap images, processed and analysed using ImageJ software [32], which has in-built functionality for calculating the fibre volume fractions. The measurements were made based on five images for each type of tow, and the determined values are specified in Table 1, along with the fibre count in the tow and the filament diameter.

As was argued in subsection 2.2, all the parameters associated with a tow can be lumped into a single controllable property, its cross-sectional area, using Eq. (9). Two tow cross-sections, the weft and the warp, along with the tow densities in the weave, namely, p_{weft} , p_{warp} and H_{UC} , form a complete set of parameters for the designer to work with. These are the parameters that can be controlled in manufacturing, directly or indirectly. In general, practicality of the designable parameters is a crucial consideration that must be accounted for when selecting the designable parameters. It helps to bridge the gap between the designers and the manufacturers by facilitating a dialogue between them.

 Table 1

 Controllable parameters for the benchmark composite configuration.

Topological parameters [26]		Controllable parameters				
		Parameters associated w	Parameters associated with the weave			
		•	warp	weft	'	
n _{step}	1	Filament count [26]	12 K	12 K	$p_{weft}, \ { m cm}^{-1}$	2.4
n _{skip}	1	Average filament diameter, µm [31]	5	5	p_{warp} , cm ⁻¹	7
n _{steep}	2				H _{UC} ,mm [26]	0.41
n_{deep}	2	Intra-tow fibre volume fraction (SD) Measure of roundness of cross-section [26]	0.75 (0.01) 0.05	0.72 (0.02) 0.5		

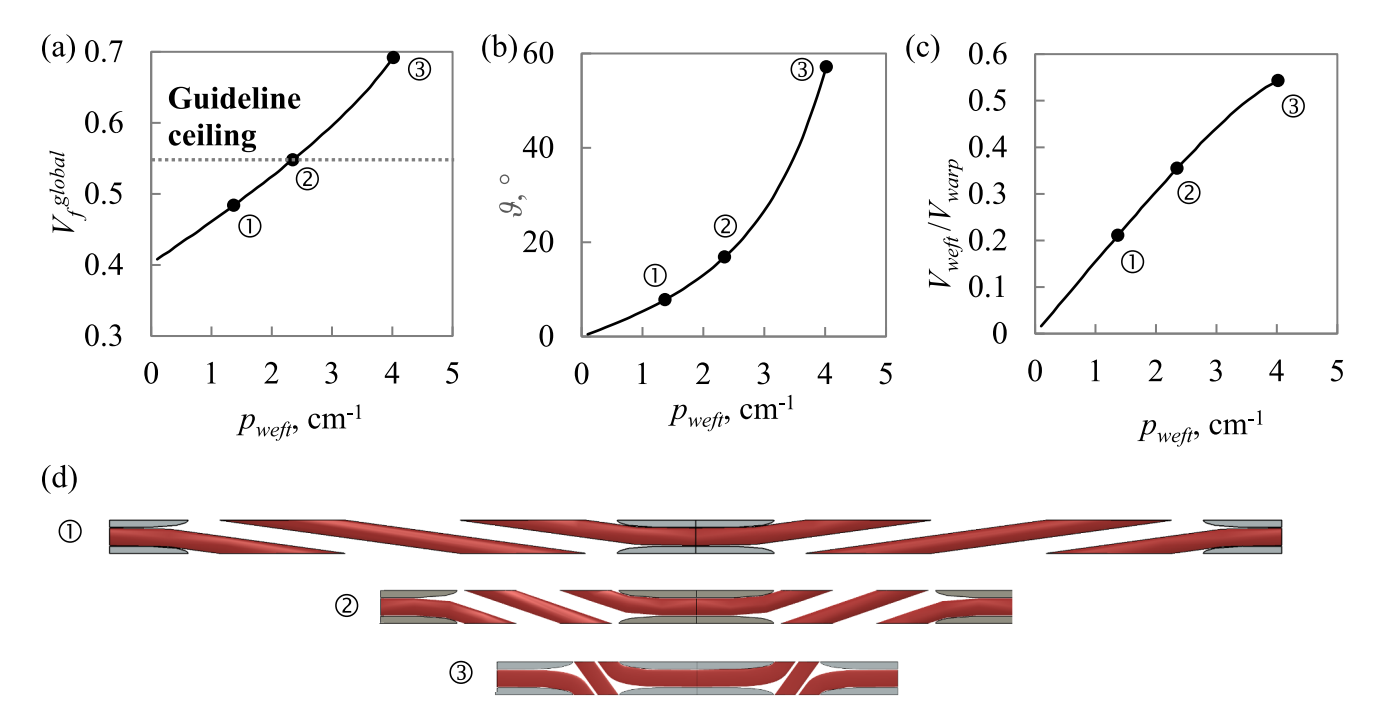


Fig. 4. Variation geometric properties with the weft tow density: (a) global fibre volume fraction; (b) the interlocking angle and (c) tow ratio. Plot (d) — geometry of the UC at different weft tow densities.

3.3. Tow density variation schemes

When designing woven composite, the first basic consideration is to ensure that the global fibre volume fraction is sufficiently high. Using its derived expression (12), V_f^{global} has been plotted as function of p_{weft} in Fig. 4(a), along with the interlocking angle and the tow ratio that are plotted in Fig. 4(b) and (c) for completeness of presentation, while keeping the remaining controllable parameters and properties fixed. All these calculations were carried out using the MATLAB script [30].

As can be seen, all three KPoWs increase monotonically with p_{weft} . The critical value of p_{weft} , that corresponds to the tightest packing of the tows, has been derived analytically in and its expression is given in the Supplementary file document. The variations in geometry of the UC associated with the variation of p_{weft} are illustrated in Fig. 4(d). It is easy to see that as p_{weft} increases, the weft tow columns move closer together and the resin-rich areas shrink, thus resulting in higher fibre volume fraction. The warp tow undulations become steeper, leading to higher interlocking angle. At the tightest packing of the weft tows, corresponding to configuration ③ as marked in Fig. 4, the maximum of the global fibre volume fraction is nearly 0.7, and the interlocking angle is

just under 60° , both of which are rather extreme. Based on the global fibre volume fractions estimates from [26] and [13], it is reasonable to take $V_f^{global}=0.55$ as a sufficiently high volume fraction achievable in most woven composites. This limit, that will be referred to as the 'guideline ceiling' value of V_f^{global} is marked by a dotted grey line in Fig. 4 (a). Having set this restriction, the value of $p_{weft}=2.4~{\rm cm}^{-1}$ corresponding to $V_f^{global}=0.55$ has been chosen as the benchmark value.

The monotonic dependency of the global fibre volume fraction on the p_{weft} signifies that to retain the same global fibre volume fraction while varying the p_{weft} , at least one other controllable parameter should be changed simultaneously. In general, change in any controllable parameter leading to the tighter weave packing should be compensated by an appropriate change in a different controllable parameter that would cause loosening of the weave. Based on this consideration, three variations schemes involving three tow densities, p_{weft} , p_{warp} and H_{UC} , can be defined. In each scheme, one tow density is kept constant, while the other two change in a way that ensures the constancy of the global fibre volume fraction.

Variations of the tow densities associated with each variation scheme

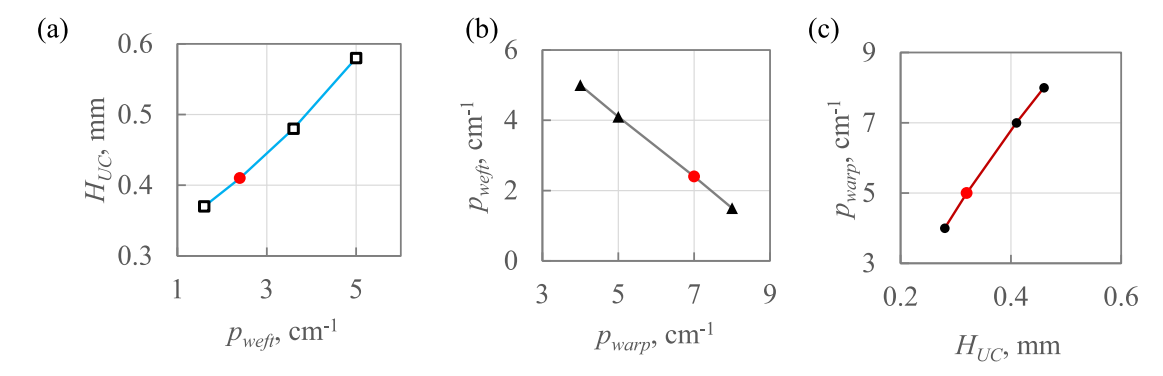


Fig. 5. Tow density variation schemes: (a) p_{weft} and H_{UC} varied while $p_{warp,b} = 7 \text{ cm}^{-1}$; (b) p_{weft} and p_{warp} varied while $H_{UC,b} = 0.41 \text{ mm}$; (c) H_{UC} and p_{warp} varied while $p_{weft,b} = 2.4 \text{ cm}^{-1}$. Benchmark values are shown as a red circle symbol. (For interpretation of the references to colour in this figure legend, the reader is referred to the web version of this article.)

are shown in Fig. 5. To expose the relationship between p_{weft} and H_{UC} in Fig. 5(a), first, set of four discrete values of p_{weft} , including its benchmark value from Table 1, was chosen. At each value of p_{weft} , controllable parameter H_{UC} was altered manually until $V_f^{global}=0.55$ was reached, while all the remaining controllable properties and parameters, including p_{warp} , were kept fixed at their benchmark values, which henceforth will be denoted by a subscript 'b'. Same procedures have been followed to obtain variation of p_{weft} relative to p_{warp} in Fig. 5(b) and that of p_{warp} relative to H_{UC} in Fig. 5(c). These calculations have been carried out in MATLAB script [30]. As can be seen, all three relative variations of the tow densities are monotonic and consistent in a sense that they are to an opposite effect, one causing tightening of the weave while the other compensating it by loosening the weave.

It is worth noting that the mechanism of variation of H_{UC} may seem to be unclear, because, unlike the weft and the warp tow densities, it is not a conventional parameter on its own. However, as was explained earlier, it is directly associated with the thickness of the composite panel, which can be controlled in manufacturing by the height of the cavity in the mould tool. Then the tow density variation where H_{UC} is constant (as Fig. 5(b)) implies that the thickness of the panel would not change while the weave geometry is varied. The other two schemes, where H_{UC} is varying, naturally imply that the thickness of the panel is allowed to change as the designable parameter.

Variations of tow densities in Fig. 5 were obtained while keeping one of the KPoWs, the global fibre volume fraction, constant at $V_f^{global} = 0.55$. However, the interlocking angle, ϑ , and the tow ratio, V_{weft}/V_{warp} , were not restrained in any way. Establishing trends in their variation relative to the tow densities is key to establishing the design method in the present paper.

Making use of three tow density variation schemes, ϑ and V_{weft}/V_{warp} have been obtained as plotted in Fig. 6. Specifically, considering them as functions of p_{weft} and p_{warp} that are related as shown in Fig. 5(b), values of these KPoWs were calculated for each pair (p_{weft}, p_{warp}) using Eq. (11) and Eq. (13). The obtained interlocking angle and tow ratio were plotted against p_{weft} in Fig. 6(a) and (d), respectively, and, for completeness of

presentation, they were also plotted as functions of p_{warp} in Fig. 6(b) and (e), where they are marked by the same black triangle symbols.

In a similar way, variation of the KPoWs was obtained where the varying controllable parameters were p_{weft} and H_{UC} (shown as hollow square symbols in Fig. 6(a), (d), (c) and (f)), while the black circle symbols illustrate variations of KPoWs brought about by tow density variation scheme involving H_{UC} and p_{warp} .

Considering variations of the interlocking angle and the tow ratio in Fig. 6, following important observations can be made:

- For each tow density variation scheme, both the interlocking angle and the tow ratio change monotonically. This offers great convenience for design exercises, because qualitatively, the trend of variation of tow densities on KPoWs will always be predictable.
- 2) The interlocking angle and the tow ratio cannot be varied independently. If one of the varying controllable parameters is p_{weft} both ϑ and V_{weft}/V_{warp} would increase with p_{weft} as shown in Fig. 6(a) and (d), respectively. In other words, the denser the packing of the weft tows, the larger is the interlocking angle and the larger is the weft tow volume fraction. If p_{weft} was kept fixed, the interlocking angle and the tow ratio will follow the opposite trends, as plotted in Fig. 6 (b) and (e) (or, equivalently, Fig. 6(c) and (f)), respectively.
- 3) Varying tow densities alone could suffice to produce significant variation in both θ and V_{weft}/V_{warp} .

Before proceeding with development of the design method, it is important to clarify the role of the tow cross-sectional areas A_{weft} and A_{warp} . Their influence on the KPoWs can also be explored computationally, if desired, because they are involved, directly or indirectly, in definition of all three KPoWs given by Eqs. (10), (12) and (13). However, treating these two controllable properties the same way as the tow densities, namely, involving them in variation schemes, could make the design unmanageable, because it would increase the number of combinations of the controllable parameters and the controllable properties. One helpful consideration to take into account is that selection A_{weft} and A_{warp} has no effect on the trends in variation of the KPoWs associated

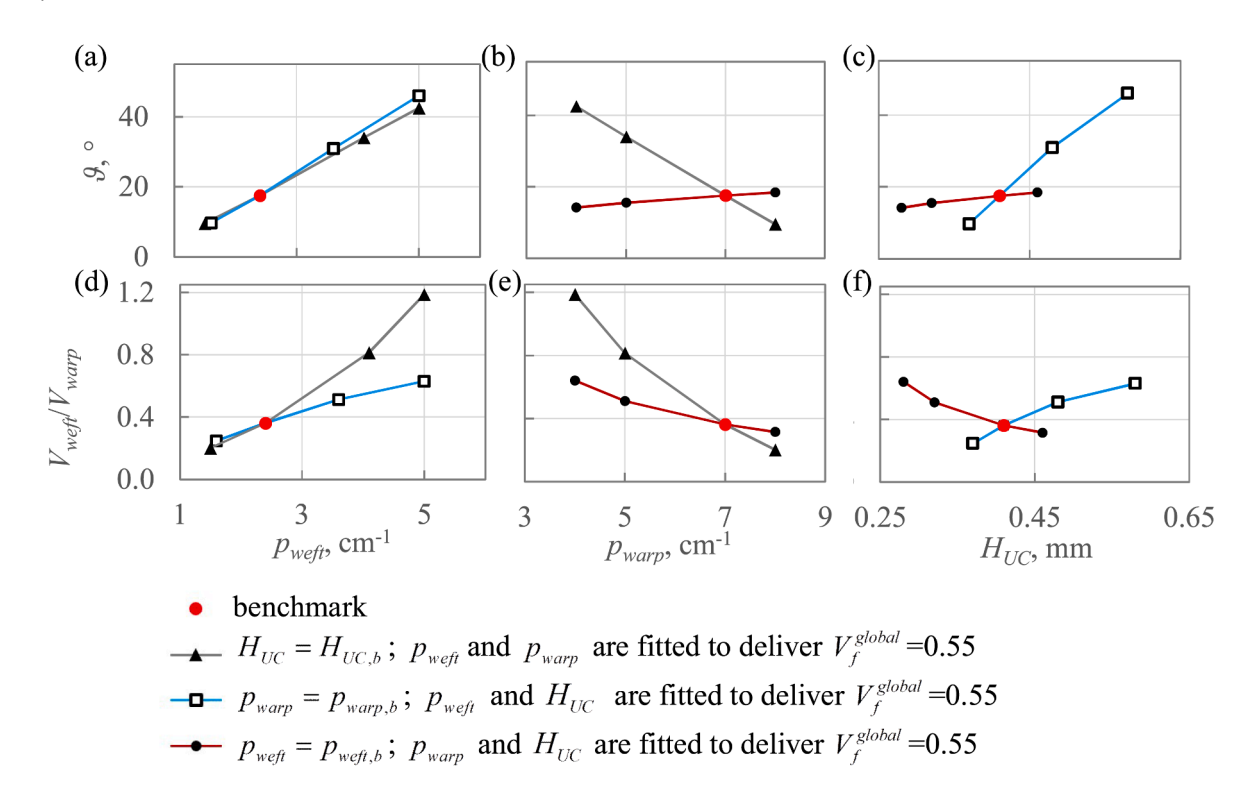


Fig. 6. Variation of KPoWs with respect to the tow densities: (a), (b), (c) interlocking angle; (d), (e), (f) tow ratio.

with different tow density variation schemes. Specifically, the analyses as presented above have been repeated for a composite configuration with 6K filaments in the warp and 24K filaments in the weft tows, which is substantially different from the benchmark configuration. While the obtained values of KPoWs were different from those in Fig. 6, the variation trends the KPoWs followed at three tow density variation schemes were identical to those presented in Fig. 6. The role of the tow cross-sectional areas in composites design will be elaborated in a separate publication.

4. Design for the mechanical performance via geometry variation

In the previous section, the KPoWs were related to controllable parameters by associating trends in their variation to three tow density variation schemes. Having established this link, one can competently vary the controllable parameters to obtain the desired combinations of the KPoWs. At the same time, the KPoWs are known to affect the mechanical behaviour of the woven composites. However, understanding of the association between the KPoWs and the mechanical properties has never been systematic. In this section, the nature of association between the KPoWs and the elastic properties of the woven composites will be elaborated.

4.1. Material characterisation tool and data

The elastic characterisation was carried out based on unit cell model full details of which are given in [27]. As has been mentioned earlier, the model was extensively validated against the experimental data in [26]. The material characterisation in [26,27] has been fully automated using the Python script. The same script was used to obtain all the results below, with the only difference that all the geometry-related input is now defined in terms of the controllable parameters.

In total, 10 composite configurations have been characterised, one being the benchmark configuration, and the remaining covering three tow density variation schemes as have been detailed in subsection 3.3. The values of tow densities corresponding to different variation schemes can be read from Fig. 5. The second set of the input properties were the properties of constituents, namely, the matrix and the fibre tows. The latter were determined from the micro-scale characterisation employing the UnitCells© tool [33] following the procedure previously detailed in [26]. The input properties of constituents are summarised in Table 2 and they were kept constant in all characterisation cases.

4.2. Variation of the effective elastic properties

Each material characterisation conducted delivered a complete set of the effective elastic properties. The effective elastic and shear moduli have been plotted against the interlocking angle and the tow ratio in Fig. 7. Three different types of symbols refer to the respective tow density variation schemes as were established in subsection 3.3. For example, triangle symbols refer to the variation schemes shown in Fig. 5 (b), in which the weft and the warp tow densities change, while the

height of the unit cell is kept constant. The interlocking angle and the tow ratio associated with such tow density variation increase or decrease simultaneously, as shown in Fig. 6, where their respective values are also marked by the triangle symbols. Each of three material configurations associated with this variation scheme has been characterised, and the same effective stiffness values were plotted both against the interlocking angle and against the tow ratio in Fig. 7. The other two sets of characterisation results are to be related to their respective tow density variation schemes in the same way.

The characterisation results in Fig. 7 show two clear global variation trends of the direct effective stiffnesses. The first one is the increase in the weft effective modulus, E_2 , with the tow ratio in Fig. 7(d). It simply means that the higher the volume fraction of the weft tows (and hence the tow ratio), the larger the effective weft Young's modulus. The second distinctive trend is the reduction of the warp Young's modulus, E_1 , with the interlocking angle, as shown in Fig. 7(a). This is consistent with the common perception that large undulations of the warp tow cause reduction in the warp stiffness [8,35]. However, according to the trends in variation of KPoWs established in subsection 3.3, the interlocking angle and the tow ratio increase simultaneously in such cases. Therefore, the warp stiffness reduction is in fact due to a combined effect of the reduced warp tow volume fraction and the large interlocking angle. The simultaneous increase in the weft Young's modulus and the reduction of warp Young's modulus for layer-to-layer angle interlock composite have also been reproduced, both numerically and experimentally, in [21], where the association between the weft tow volume fraction and the weft stiffness, and that between the interlocking angle and the warp stiffness has also been identified. However, in [21], the variation of the weft tow volume fractions was realised merely by changing the number of filaments in the weft tows, implying that the tow volume fraction is deemed to increase with its size. This, in fact, reflects a common perception that the tow volume fractions, and therefore the tow ratio, should be controlled by the sizes of the tows, while the tow density mostly affects the spacing between the tows and hence the interlocking angle. The results presented in Fig. 6 and Fig. 7 testify that this is by far not universally applicable, namely, the weft tow volume fraction can change over a wide range while the tow size is kept fixed.

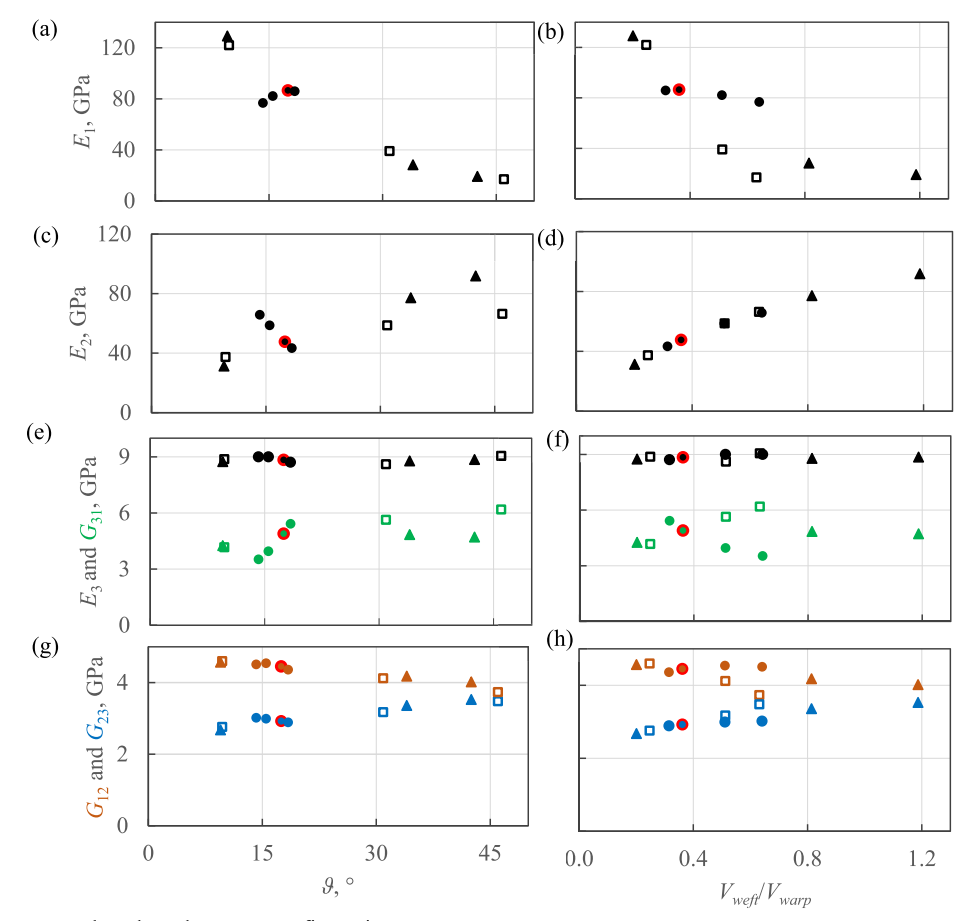
Equipped with understanding of trends in variation of KPoWs, the counterintuitive local increase of warp stiffness with the interlocking angle in Fig. 7(a) can be explained. The variation of the KPoWs associated with this localised effect is realised through the tow density variation scheme where p_{weft} is kept fixed. In such case, the increase in the interlocking angle is accompanied by a reduction of the tow ratio, as can be seen in Fig. 6(b) and (e). This means that the warp tow volume fraction increases simultaneously with the interlocking angle, which are the two competing trends as far as their effects of the warp stiffness are concerned. Therefore, the detrimental effect on the warp stiffness from ϑ , as it increases, is alleviated by warp tow volume fraction that follows the same trend, to such extent that it even causes a marginal increase in the warp stiffness.

Compared to the two in-plane effective elastic moduli, the remaining properties show little to no variation with respect to the KPoWs. The through-the-thickness effective elastic modulus, E_3 , is substantially

Table 2 Properties of the constituent materials.

ACTECH 1304		TZ800H fibres		TZ800H tows	TZ800H tows		
				Weft tow, 72(76)%*	Warp tow, 75(82)%*		
E, GPa	3.53[34]	E ₁ , GPa	294[31]	224.01	241.42		
ν	0.35	$E_2 = E_3$, GPa	15	10.12	11.11		
		$ u_{12}= u_{13}$	0.28	0.295	0.291		
		v_{23}	0.35	0.405	0.393		
		$G_{12}=G_{13}$, GPa	15	6.04	7.406		
		G_{23} , GPa	5.55	3.60	3.987		

^{*} Reasons for scaling of the intra-tow volume fraction have been justified and elaborated in [26].



- benchmark weave configuration
- ▲ tow density variation scheme as in Figure 5 (b)
- tow density variation scheme as in Figure 5 (a)
- tow density variation scheme as in Figure 5 (c)

Fig. 7. Effective elastic properties as functions of the interlocking angle (plots(a),(c),(e) and (g)) and tow ratio (plots(b),(d),(f) and (h)).

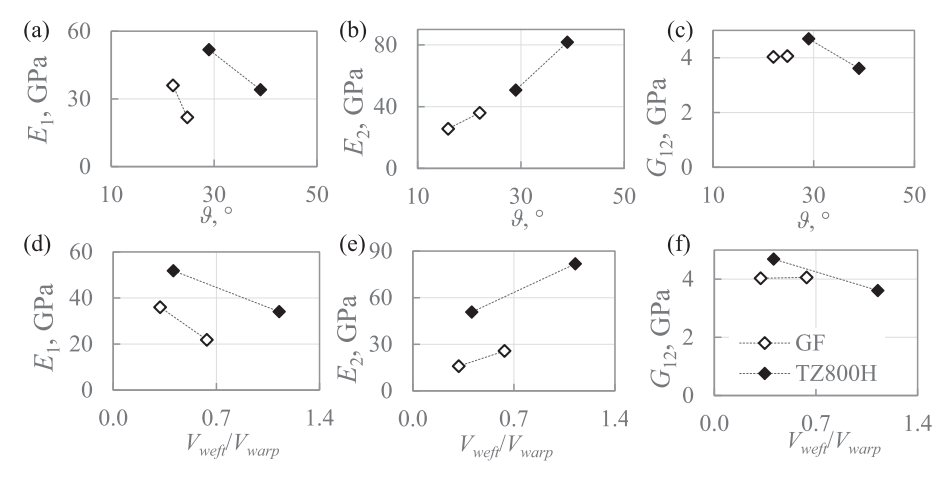


Fig. 8. Variation of the effective elastic properties with the KPoWs captured experimentally: (a),(d) – effective elastic modulus along the warp direction; (b),(e) – effective elastic modulus along the weft direction; (c),(e) – effective in-plane shear modulus.

lower than the in-plane ones and is essentially insensitive to variations in geometry, as can be seen in Fig. 7(e) and (f). Low in-plane shear stiffness, G_{12} , is a known generic weakness of the woven fabric due to orthogonal arrangement of the fibre tows. As the characterisation results show, same is true for G_{23} . Both show only weak tendency to reduce and

increase, respectively, with respect to both KPoWs, as shown in Fig. 7(g) and (h). Among all the effective shear moduli, G_{31} has the largest design potential, as it shows reasonably substantial scatter as the KPoWs vary, as can be seen in Fig. 7(e) and (f). However, it is lacking global distinctive variation trends, which makes its design more challenging.

Table 3 Composite configurations and KPoW corresponding to different n_{steep} .

Notation	$n_{steep} = n_{deep}$	$p_{weft}, \ { m cm}^{-1}$	$p_{warp}, \ { m cm}^{-1}$	$H_{UC},$ mm	θ, °	V_{weft}/V_{warp}
benchmark	2	2.4	7	0.41	17.5	0.36
C1	3	2.2	7	0.41	23.0	0.32
C2	3	2.4	7	0.42	26	0.35
C3	4	2	7	0.41	26.4	0.29
C4	4	2.4	7	0.44	33.2	0.33

Trends in variation of the effective properties with the KPoWs as exposed above can also be reproduced utilising measured effective elastic properties and calculated KPoWs reported in [26]. Two sets of composites, one based on glass and another on carbon fibre 3D woven reinforcement, had the same constituents within each set, yet significantly different internal geometries which resulted in different effective elastic properties. Plotting them against the KPoWs in Fig. 8, trends in variation of the elastic properties are consistently reproduced.

5. Contribution of the topological parameters

Same as the controllable parameters, the topological parameters influence the effective elastic properties. The parametric studies with respect to all the topological parameters have been reported in [27] and in [36]. While the geometries of the reinforcements in these two studies were substantially different in terms of the KPoWs, trends in variation of the effective elastic properties with respect to topological parameters were reproduced identically, signifying that the effects from the topological parameters are decoupled from those associated with the controllable parameters.

5.1. Topological parameters associated with the warp tow path

Topological parameters n_{skip} , n_{steep} and n_{deep} define the topology of the path of the warp tow. Parametric studies [27,36] have shown that the effective elastic properties are virtually insensitive to n_{deep} . Explicit expressions of KPoWs given by Eqs. (11), (12) and (13) offer justifications for this, because none of them involves n_{deep} . This signifies that in the design exercises, parameter n_{deep} alone does not bring about any significant change in the effective elastic properties.

Topological parameter n_{skip} is involved in the expressions of tow ratio (13) and global fibre volume fraction (12) through the property k (14). It can easily be shown that

$$\lim_{n_{skip}\to\infty} k(n_{skip}) \to 1,\tag{19}$$

which implies that V_f^{global} (12) has a lower bound, while the tow ratio (13) has an upper bound. At arbitrary n_{skip} , they would not deviate too far from their respective bounds and can usually be considered reasonably constant. The third KPoW, the interlocking angle, is not affected at all, because n_{skip} is not involved in Eq. (11). Despite lack of variation in KPoWs with respect to n_{skip} , its influence on effective properties was not negligible [27,36], because presence of straight stretches of the warp tows at high values of n_{skip} brought about the increase in E_1 and

reduction in G_{31} , that were the only two effective properties noticeably affected.

Parameter n_{steep} is directly involved in expressions associated of all three KPoWs (11)-(14), which show wide range of variations with n_{steep} [27,36]. The interpretation of the effect of n_{steep} on the construction of the weave is straightforward: the larger the value of n_{steep} , the more warp tows should be accommodated in the space between the two adjacent weft tows, e.g. three warp tows in Fig. 1 and Fig. 2(b), or two warp tows in Fig. 2(a), which results in denser packing. Therefore, to maintain practical V_f^{global} , at least one controllable parameter should be adjusted accordingly, following the same logic as was employed when introducing tow density variation schemes in subsection 3.3. To assess to what extent n_{steep} can influence the KPoWs and the effective elastic properties, effective properties of five composite configurations as detailed in Table 3 were produced. For each of them, to keep $V_f^{global} = 0.55$, one of the controllable parameters was changed along with n_{steep} , while the remaining parameters were kept at their benchmark values.

Characterisation revealed that only E_1 , E_2 and G_{31} vary distinctively with KPoWs as shown in Fig. 9. Their variation trends are identical to those established in the previous section. Note that E_2 variations are substantially smaller those of E_1 and G_{31} , because the tow ratio, which controls the E_2 , is a lot less sensitive to variation of n_{steep} than the interlocking angle is, as can be seen in Table 3. Therefore, it is natural to expect that the weft elastic modulus would vary substantially less than the warp one. It can be concluded that n_{steep} can serve as effective means of simultaneously reducing E_1 and increasing G_{31} . This is exactly opposite to variation of the same properties with respect to n_{skip} .

5.2. Anisotropy considerations

The remaining topological parameter, n_{step} , defines the extent to which the adjacent warp tows are shifted relative to each other, as is shown in Fig. 2. It is not involved in expressions for any of KPoWs, but was shown in [27,36] to cause increase in both E_1 and G_{31} .

The special significance of parameter n_{step} is that its certain choices could alter the characteristics of symmetries present in the woven composite. The reflectional and rotational symmetries help to identify the extent of material anisotropy [30]. The categorisation of materials in terms of their anisotropy is of great practical importance, because all the existing testing standards are for materials that are at least orthotropic. From the manufacturing side, the components made of highly anisotropic composites can become warped after manufacturing due to coupling between the direct and the shear stresses.

The topology of composites analysed in previous sections delivers orthotropy because there exist two perpendicular axes of rotational symmetry [29], as marked in Fig. 2(c). In general, the orthotropy will be realised in configurations where the adjacent warp tows are shifted relative to each other by the half length of the unit cell, as is illustrated in Fig. 10 with $n_{step}=2$. The consequence of the lack of reflectional or rotational symmetries can be exposed when considering the full compliance matrix that is the one of the outputs of the conventional characterisation exercise [29]. For composite shown in Fig. 10 with $n_{step}=1$ the compliance matrix has been calculated as

$$S|_{\eta_{\text{step}}=1} = \begin{pmatrix} 0.204 & -0.004 & -0.087 & 4 \times 10^{-6} & -0.6 \times 10^{-6} & -80 \times 10^{-6} \\ -0.004 & 0.095 & -0.053 & -2 \times 10^{-6} & 0.2 \times 10^{-6} & 0.002 \\ -0.087 & -0.053 & 1.107 & -1 \times 10^{-6} & 4 \times 10^{-6} & -0.0005 \\ 4 \times 10^{-6} & -2 \times 10^{-6} & -1 \times 10^{-6} & 2.878 & 0.023 & -20 \times 10^{-6} \\ -0.6 \times 10^{-6} & 0.2 \times 10^{-6} & 4 \times 10^{-6} & 0.023 & 3.488 & -2 \times 10^{-6} \\ -80 \times 10^{-6} & 0.002 & -0.0005 & -20 \times 10^{-6} & -2 \times 10^{-6} & 2.166 \end{pmatrix} \times 10^{-4} \text{MPa}^{-1}$$
 (20)

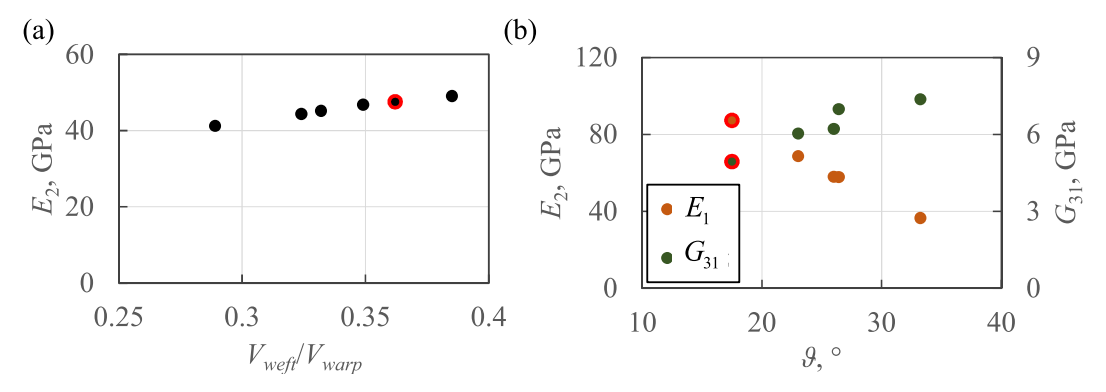


Fig. 9. Effective properties with associated with variation of n_{steep} : (a) weft stiffness, E_2 , as function of tow ratio; (b) E_1 and G_{31} as functions of the interlocking angle.

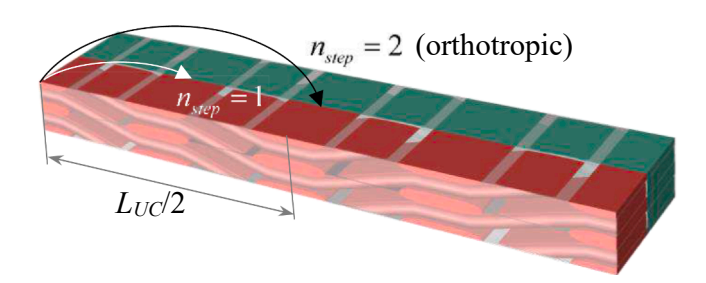


Fig. 10. Definition of parameter n_{step} in configuration with $n_{skip} = n_{steep} = 1$ and $n_{deep} = 2$.

For the orthotropic material, all the off-diagonal 3×3 submatrices should vanish, Computationally, they are typically shown as numbers several orders of magnitude smaller than those along the diagonal of the matrix. This signifies absence of interaction between direct and shear stresses and strains. Equally, in the lower right 3×3 submatrix, all off-diagonal elements should vanish to prevent any interaction among shear stresses themselves. Since the material under consideration only had one useful (rotational, in this case) symmetry, there are several non-trivial elements indicating coupling effects. The material can be categorised as being monoclinic with the only principal axis in the through-thickness direction. The parametric studies with respect to n_{step} in [27,36], while not addressing the matter of anisotropy, have shown that the maxima of E_1 and G_{31} are reached in the orthotropic arrangement.

At present, there is the lack of systematic understanding of anisotropy and its effect on mechanical performance in wider composites community. For example, while composite configuration analysed in [21] was topologically identical to that in Fig. 10 with $n_{step}=1$, lack of orthotropy and its implications have not even been mentioned there. This is not to imply that composite configurations bearing higher degrees of anisotropy should be avoided altogether. However, effect of anisotropy on the mechanical behaviour of the material should be carefully assessed, so that an informed decision can be made regarding

the applicability of such material in practical design.

6. Application of KPoWs in a design of a 3D woven composite

6.1. Complete design cycle

The design cycle for 3D woven composites design is schematically illustrated in Fig. 11. A version of the same scheme presented in [26] implied that the controllable parameters should be employed explicitly in design exercises. As was argued earlier, direct use of controllable parameters would be highly impractical, because there are too many of them and there is no direct association between them and the mechanical properties of the composites.

Use of KPoWs as an intermediate stage of design offers an effective alternative to the direct use of controllable parameters. The KPoWs have been related to the controllable parameters in Section 3 by determining the trends in their variation relative to the controllable parameters and relative to each other. At the same time, the variation trends of the effective elastic properties with respect to the KPoWs and the topological parameters of the weave were established in Sections 4 and 5, respectively. Basically, through KPoWs, the controllable and the topological parameters have been associated with the effective elastic properties. In view of this, calculation of KPoWs becomes a crucial step of the design. The KPoWs are calculated outside the material characterisation routine, utilising MATLAB script. Appropriate tow density variation schemes are followed to achieve the desired change in KPoWs. The computationally demanding material characterisation based on FE modelling is only used at the advanced stage of a design process.

It is worth noting that when carrying out the design exercise, the material characterisation tool does not necessarily have to be the unit cells in their FE implementation. If an alternative method is mathematically and mechanically consistent, it is reasonable to expect that the trends in variation of the KPoWs, and those of the effective elastic properties should be reproduced, even though quantitatively the results may differ. The advantage of the unit cells is that they strike a balance between the accuracy of predictions they deliver and the practicality, especially after the unit cells modelling tool has been automated and

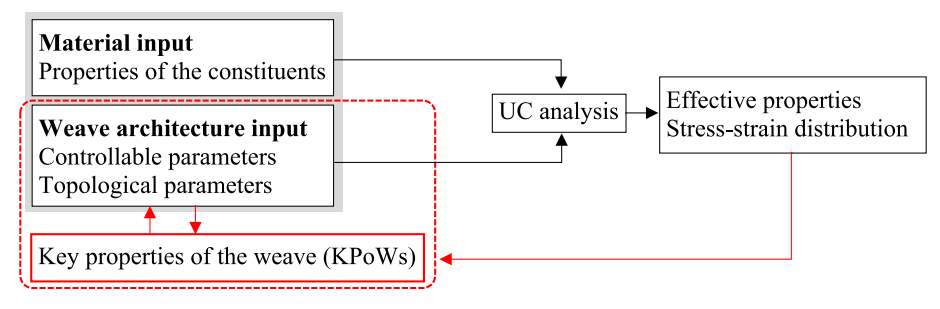


Fig. 11. Complete design cycle for a 3D woven composite.

Table 4Design for the balanced arrangement.

	Input					MATLAB	calculations		UC characterisation	
	p_{weft} , cm ⁻¹	p_{warp} , cm ⁻¹	H_{UC} , mm	A_{weft} , mm ²	A_{warp} , mm ²	θ, °	$rac{V_{weft}}{V_{warp}}$	$V_{f,global}$	E ₁ , GPa	E ₂ , GPa
Initial	2.4	7	0.41	0.31	0.29	17.5	0.36	0.55	87.3	47.61
Iteration 1	3.3	7	0.46	0.31	0.29	27.5	0.48	0.55	48.24	56.54
Iteration 2	3.1	7	0.45	0.31	0.29	25.2	0.45	0.55	55.36	54.56

made openly accessible [29]. They allow for straightforward derivation of KPoWs as functions of controllable parameters, which could be a lot more demanding and/or less practical if an alternative characterisation method is used. The unit cell modelling may indeed introduce some systematic inaccuracies in predictions because of idealisation of the weave architecture. However, in design, trends in variation of the properties prevail over the demand on high numerical accuracy of predictions. Sophisticated models incorporating numerous localised varying features of the woven reinforcement may deliver more accurate predictions, but their use in design will inevitably amplify the number of the properties and parameters to account for, which can make the design cycle simply impractical. Problem of accuracy of predictions can be addressed at the advanced stages of material selection process, where use of highly accurate predictive models would be fully justified.

6.2. Example of application

Consider design of a balanced composite configuration, in which the weft and the warp effective moduli are of the same magnitude. The first step of the design is selection of an initial composite configuration. Without loss of generality, consider the benchmark configuration defined by controllable parameters from Table 1 as the initial one. The complete set of input controllable parameters, the calculated KPoWs and

the two effective properties being designed are summarised in Table 4. As can be seen, for the initial configuration, the weft effective elastic modulus is around half the warp one. For balanced arrangement, one needs to bring the former up and the latter down. To achieve this, the tow ratio and the interlocking angle should be both increased. As has been elaborated in subsection 3.3, this can be realised through either of the two tow density variation schemes where one of the varying parameters is p_{weft} , and in the present example, tow density variation scheme involving p_{weft} and H_{UC} will be used. Following this scheme, the interlocking angle and the tow ratio will both increase with p_{weft} . Having increased p_{weft} , to maintain V_f^{global} at a guideline ceiling level, which in

this case is $V_f^{ceiling}=0.55$, one also needs to increase H_{UC} accordingly. To obtain the appropriate value of H_{UC} , several iteration are carried out using the MATLAB script [30]. This stage of design is the process marked by the red dashed rounded rectangle in Fig. 11. As a result, a set of the input parameters denoted as 'Iteration 1' in Table 4 is obtained. Next, material characterisation is carried out to check how close the effective moduli are to the target values. This is an advanced stage of design, involving unit cell characterisation, which is also specified in Fig. 11. As can be seen, the change is as expected; overall, effective elastic moduli are much closer to the design objective than in the 'Initial' case, but the

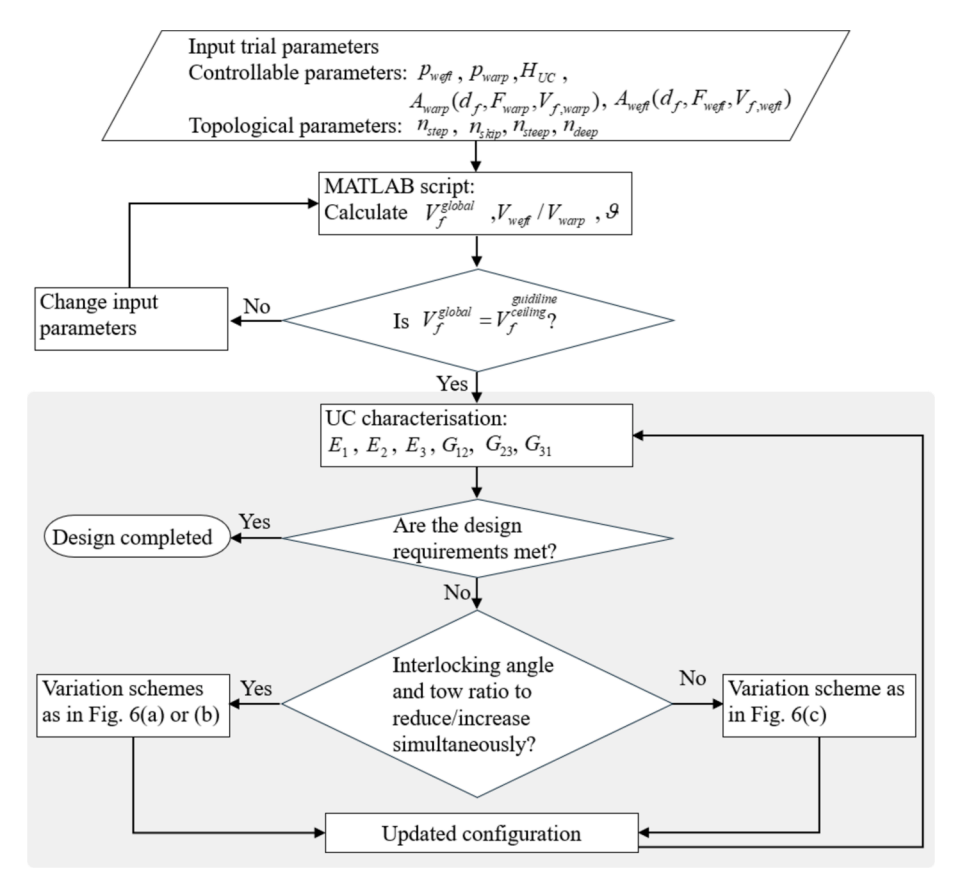


Fig. 12. Detailed scheme for design via the tow density variation.

weft modulus is now larger than the warp one. To correct this, design returns to the previous stage, where values of p_{weft} and H_{UC} are slightly reduced while keeping $V_f^{global}=0.55$. The resultant configuration, denoted as 'Iteration 2' in Table 4, happens to be of an almost balanced arrangement. If the disparity between the two directions is still to be narrowed down, the iterations as described above can be continued.

Note that the controllable parameter variation procedure can be automated to some extent by replacing the manual adjustment of the

guildiline

tow densities to achieve $V_f^{ceiling}=0.55$ by an iteration scheme. At the same time, the manual adjustment procedure is not overly demanding, because there exist some practical restrictions on how the designable parameters can be varied. Specifically, the variation of the tow densities is incremental, not continuous. Because of that, there are very few combinations of tow densities the user can try, and the desired combination can usually be achieved in 3–4 iterations.

The design scheme followed in this exercise is shown in Fig. 12. In its entirety, it describes the design process where the initial choice of the parameters is completely random. In the example above, a valid composite configuration with known mechanical properties has been used as the starting point, therefore the design process in this case was as marked by shading in Fig. 12. Note that variation of the KPoWs via variation of the topological parameters, as was explained in Section 5, while not used in this design exercise, is certainly a valid alternative to tow density variation and can replace it in the design process, if topology variation is the preferred method of design.

7. Conclusions

A practical scheme for design of the elastic properties of 3D woven composites has been formulated, delivering a much-needed design capability for these materials. Design of 3D woven composites has been defined as an iterative procedure, like any design process, where the reinforcement architecture is varied in informed way to deliver a desired elastic behaviour of the material. Practicality of the design scheme has been ensured by employing the three key properties of the weave (KPoWs): the global fibre volume fraction, the interlocking angle and the tow ratio. These properties are calculated and assessed as an intermediate yet an essential step of the design exercise utilising a MATLAB script [30]. The nature of KPoWs is that they are related both to the controllable (associated with manufacturing) parameters and to the effective elastic properties that systematically vary with the KPoWs.

Explicitly deriving the KPoWs as functions of controllable parameters offered means for ensuring that the design would deliver only practical composite configurations. Invalid configurations were eliminated from consideration by deriving condition on critical combination of controllable parameters that corresponds to the tightest compaction of the tows in the weave. Practicality was ensured by defining the rules of variation of the controllable and the topological parameters that would keep the global fibre volume fraction at a 'guideline ceiling' value.

It is worth noting that the focus of present paper has been on the design of the elastic properties, which represent a relatively simple mechanical behaviour. However, without capability to design such basic behaviour, design of more advanced behaviours is simply not possible. With the elastic behaviour under control, designers are now in position to explore more advanced design objectives, e.g. strength. Also, the design capability has been established for 3D woven composites of layer-to-layer angle interlock architectures, which is a type of woven composites. However, the design philosophy adopted is not restrictive in a sense that it is applicable to any other type of textile composites.

CRediT authorship contribution statement

Elena Sitnikova: Writing - review & editing, Writing - original

draft, Visualization, Validation, Methodology, Investigation, Funding acquisition, Conceptualization. **Mingming Xu:** Software. **Weiyi Kong:** . **Shoufeng Hu:** Project administration. **Shuguang Li:** Writing – review & editing, Supervision, Funding acquisition, Conceptualization.

Declaration of competing interest

The authors declare that they have no known competing financial interests or personal relationships that could have appeared to influence the work reported in this paper.

Acknowledgements

The authors would like to thank AECC CAE, China contract number 126961 for providing financial support for this research. They also acknowledge assistance of Shuang Qin, postdoctoral researcher at the Institute of Mechanics, Chinese Academy of Sciences, Beijing, China on determining the intra-tow fibre volume fractions.

Appendix A. Supplementary data

Supplementary data to this article can be found online at $\frac{\text{https:}}{\text{doi.}}$ org/10.1016/j.matdes.2024.113414.

Data availability

The MATLAB scripts are available under DOI: 10.17632/tzhjg99wt7.2.

References

- K. Bilisik, Multiaxis three-dimensional weaving for composites: a review, Text. Res. J. 82 (7) (2012) 725–743.
- [2] Y. Wielhorski, A. Mendoza, M. Rubino, S. Roux, Numerical modeling of 3D woven composite reinforcements: a review, Composites Part A: Appl. Sci. Manuf. (2021) 106729
- [3] A. Trofimov, C. Ravey, N. Droz, D. Therriault, M. Lévesque, A review on the Representative Volume Element-based multi-scale simulation of 3D woven high performance thermoset composites manufactured using resin transfer molding process, Compos. A Appl. Sci. Manuf. 169 (2023) 107499.
- [4] S.Z.H. Shah, P.S.M. Megat-Yusoff, S. Karuppanan, R.S. Choudhry, Z. Sajid, Multiscale damage modelling of 3D woven composites under static and impact loads, Compos. A Appl. Sci. Manuf. 151 (2021) 106659.
- [5] M.N. Saleh, C. Soutis, Recent advancements in mechanical characterisation of 3D woven composites, Mech. Adv. Mater. Mod. Processes (2017), https://doi.org/ 10.1186/s40759-017-0027-z.
- [6] G. Marsh, Aero engines lose weight thanks to composites, Reinf. Plast. 56 (6) (2012) 32–35
- [7] Clarkson, E., Hexcel 8552 AS4 unidirectional prepreg qualification statistical analysis report. 2011, National Institute for Aviation Research.
- [8] A.P. Mouritz, B.N. Cox, A mechanistic interpretation of the comparative in-plane mechanical properties of 3D woven, stitched and pinned composites, Compos. A Appl. Sci. Manuf. 41 (6) (2010) 709–728.
- [9] J. Brandt, K. Drechsler, F.J. Arendts, Mechanical performance of composites based on various three-dimensional woven-fibre preforms, Compos. Sci. Technol. 56 (3) (1996) 381–386.
- [10] S. Dai, P.R. Cunningham, S. Marshall, C. Silva, Influence of fibre architecture on the tensile, compressive and flexural behaviour of 3D woven composites, Compos. A Appl. Sci. Manuf. 69 (2015) 195–207.
- [11] D.S. Ivanov, S.V. Lomov, A.E. Bogdanovich, M. Karahan, I. Verpoest, A comparative study of tensile properties of non-crimp 3D orthogonal weave and multi-layer plain weave E-glass composites. Part 2: Comprehensive experimental results, Compos. A Appl. Sci. Manuf. 40 (8) (2009) 1144–1157.
- [12] S. Dhiman, P. Potluri, C. Silva, Influence of binder configuration on 3D woven composites, Compos. Struct. 134 (2015) 862–868.
- [13] Q. Guo, Y. Zhang, D. Li, X. Sun, M. Li, L. Chen, Experimental characterization of the compressive properties and failure mechanism of novel multiaxial 3D woven composites, Compos. Commun. 28 (2021) 100905.
- [14] I.A. Abu Bakar, O. Kramer, S. Bordas, T. Rabczuk, Optimization of elastic properties and weaving patterns of woven composites, Compos. Struct. 100 (2013) 575–591.
- [15] X.-Y. Zhou, X. Ruan, S. Zhang, W. Xiong, Z. Ullah, Design optimization for thermal conductivity of plain-woven textile composites, Compos. Struct. 255 (2021) 112830.
- [16] M. Esmaeeli, M.R. Nami, B. Kazemianfar, Geometric analysis and constrained optimization of woven z-pinned composites for maximization of elastic properties, Compos. Struct. 210 (2019) 553–566.

- [17] X. Liu, X.-Y. Zhou, B. Liu, C. Gao, Multiscale modeling of woven composites by deep learning neural networks and its application in design optimization, Compos. Struct. 324 (2023) 117553.
- [18] K. Morioka, Y. Ohtake, H. Suzuki, Y. Nagai, H. Hishida, K. Inagaki, T. Nakamura, F. Watanabe, 3D woven composite design using a flattening simulation, Comput. Aided Des. 81 (2016) 24–38.
- [19] G. Pierreux, D. Van Hemelrijck, T.J. Massart, Automated generation of 3D orthogonal woven composites RVEs including yarn cross-section variations, Compos. Sci. Technol. 176 (2019) 90–102.
- [20] M. Li, K. Liu, J. Ge, J. Xie, Z. Liu, B. Zhang, J. Huang, J. Liang, A novel modeling method for the mechanical behavior of 3D woven fabrics considering yarn distortion, Compos. Sci. Technol. 230 (2022) 109691.
- [21] Z. Liu, J. Ge, K. Liu, M. Li, B. Zhang, H. Wang, J. Huang, J. Liang, High-fidelity modeling of 3D woven composites considering inhomogeneous intra-yarn fiber volume fractions, Compos. Struct. 290 (2022) 115505.
- [22] B. Wang, G. Fang, H. Wang, J. Liang, F. Dai, S. Meng, Uncertainty modelling and multiscale simulation of woven composite twisted structure, Compos. Sci. Technol. 217 (2022) 109118.
- [23] R.M. Jones, Mechanics Of Composite Materials, CRC Press, Boca Raton, 1998.
- [24] A.C. Long, L.P. Brown, 8 Modelling the geometry of textile reinforcements for composites: TexGen, in Composite Reinforcements for Optimum Performance, P. Boisse, Editor. 2011, Woodhead Publishing. p. 239-264.
- [25] I. Verpoest, S.V. Lomov, Virtual textile composites software WiseTex: Integration with micro-mechanical, permeability and structural analysis, Compos. Sci. Technol. 65 (15) (2005) 2563–2574.

- [26] E. Sitnikova, M. Xu, W. Kong, S. Li, Controllable parameters as the essential components in the analysis, manufacturing and design of 3D woven composites, Compos. Sci. Technol. 230 (2022) 109730.
- [27] M. Xu, E. Sitnikova, S. Li, Unification and parameterisation of 2D and 3D weaves and the formulation of a unit cell for composites made of such preforms, Compos. A Appl. Sci. Manuf. 133 (2020) 105868.
- [28] M.N. Saleh, A. Yudhanto, P. Potluri, G. Lubineau, C. Soutis, Characterising the loading direction sensitivity of 3D woven composites: effect of z-binder architecture, Compos. A Appl. Sci. Manuf. 90 (2016) 577–588.
- [29] S. Li, E. Sitnikova, Representative volume elements and unit cells: concepts, theory, applications and implementation. 2019: Elsevier.
- [30] E. Sitnikova, Calculation of the Key Properties of the Weave 2024. Mendeley Data, doi: 10.17632/tzhjg99wt7.2.
- [31] TZ800H datasheet. 2021, Guangwei Composite Materials Co., Ltd.: https://www.gwcfc.com/index.php?case=archive&act=show&aid=337.
- [32] C.A. Schneider, W.S. Rasband, K.W. Eliceiri, NIH Image to ImageJ: 25 years of image analysis, Nat. Methods 9 (7) (2012) 671–675.
- [33] S. Li, L.F.C. Jeanmeure, Q. Pan, A composite material characterisation tool: UnitCells, J. Eng. Math. 95 (1) (2015) 279–293.
- [34] ACTECH 1304 epoxy resin datasheet. 2020: AVIC Composite Co., LTD.
- [35] Y. Mahadik, S.R. Hallett, Effect of fabric compaction and yarn waviness on 3D woven composite compressive properties, Compos. A Appl. Sci. Manuf. 42 (11) (2011) 1592–1600.
- [36] Xu, M., Design of architecture of 3D woven composites for impact resistance. PhD thesis. 2022, University of Nottingham.